

1 **Appendix A. Detailed Methods**

2 *Appendix A.1. Solid phase geochemical analyses*

3 Samples of river bank sediments and rocks were collected from across the entire study
4 site in order to constrain the elemental and isotopic composition of different lithologic end-
5 members. Sub-samples of the river bank sediments were separated using a riffle splitter and
6 powdered in a ball mill. Rock samples were disaggregated using an agate mortar and pestle
7 before being ground in a ball mill.

8 *Appendix A.1.1. Bulk XRF measurements*

9 To determine the content of non-volatile elements in the river bank sediment samples, the
10 samples were mixed in a 1:2 ratio with lithium metaborate and then doubly fused in graphite
11 crucibles at 1000°C. The twice fused glass beads were then polished and analyzed by X-ray
12 fluorescence spectroscopy (XRF) at Pomona College. A suite of 35 elements were analyzed.
13 Only measurements of Na, Ca, Mg, and Sr concentrations are discussed in this paper. The
14 stream sediment reference material STSD-2 (Environment Canada) was processed and an-
15 alyzed using the same procedure in order to check for accuracy. For all reported elements,
16 the measured values of STSD-2 agree with certified values within 10%.

17 *Appendix A.1.2. Solid phase sulfur isotope measurements*

18 Sulfide minerals within rock samples from the Kosñipata valley are present as both macro-
19 scopic crystals and veins as well as microscopic disseminated crystals. When macroscopic,
20 sulfide minerals were sampled for sulfur isotopic analyses using a diamond-coated steel drill
21 bit and analyzed without any further preparation. When microscopic, the reduced sulfur
22 compounds were converted to H_2S and precipitated as Ag_2S using the chromium reduction
23 method of Gröger et al. (2009). Briefly, the sample powders were mixed with ethanol and
24 concentrated HCl and then reacted with an acidic $Cr^{2+}Cl_2$ solution in a N_2 -flushed digestion
25 vessel. During the reaction, the digestion vessels were heated from below with a hotplate.
26 The liberated H_2S gas was passed through a condenser and bubbled through a solution of

27 $AgNO_3$ and NH_4OH in order to trap S^{2-} as Ag_2S . For each sample, approximately 1 gram
28 of powder was reacted for one hour.

29 After the reaction was completed, the Ag_2S was separated from the $AgNO_3$ and NH_4OH
30 solution by centrifugation, rinsed three times with de-ionized water (DIW; 18.2 M Ω resistiv-
31 ity), and dried overnight in an oven at 60°C. Sub-samples of both the pyrite and homogenized
32 Ag_2S powders were sent to the University of Arizona Environmental Isotope Lab where the
33 sulfur isotopic composition was measured using an elemental analyzer coupled to a gas-source
34 IRMS (ThermoQuest Finnigan Delta PlusXL). To check the accuracy and reproducibility of
35 the chromium reduction procedure, an in-house pyrite standard was processed during each
36 session and the procedure was replicated for select samples. Overall, calculated yields for the
37 standards were similar (80-90 %; based on mass of recovered Ag_2S) and the isotopic com-
38 position of the Ag_2S produced from the pyrite standard was identical, within the analytical
39 uncertainty (0.15 ‰), to the un-processed pyrite. Similarly, variability between replicate
40 sample extractions was similar in magnitude to the analytical uncertainty (± 0.2 ‰).

41 *Appendix A.1.3. Sequential river bank sediment leaches*

42 In order to selectively dissolve carbonate minerals in the river bank sediment samples,
43 a sequential leaching procedure based on the method of Leleyter and Probst (1999) was
44 used. Both ground and un-ground sediment samples were tested, but only the leaches of the
45 un-ground sediment samples were found to selectively dissolve carbonates to a degree that
46 allowed for the determination of their chemistry. For the un-ground samples, 4-6 grams of
47 sediment were separated from the total sample using a riffle splitter and then split into two
48 roughly equal aliquots that were leached separately in 50 mL polypropylene (PP) centrifuge
49 tubes.

50 During each leaching step, the sediment samples were kept at room temperature and
51 stirred by laying the tubes on a shaking table set to 200 rpm. After each leaching step, the
52 leachate was first separated from the sediments by centrifugation. The supernatant was then
53 decanted and filtered with a 0.2 μm nylon filter. Before the next leaching step, the sediment

54 samples were rinsed three times with DIW.

55 To remove soluble salts, the sediments were first leached with 10 mL of DIW for 30
56 minutes. Next, exchangeable elements were removed by leaching the sediments with 10 mL
57 of 1M NH_4Cl for 2 hours. Finally, carbonate minerals were selectively dissolved by leaching
58 the sediments for 5 hours with 10 mL of a 1M acetic acid solution that was set to a pH of
59 ~ 4.5 by titration with NH_4OH .

60 After filtration, the acetic acid leachates were evaporated to dryness in PP vials in a
61 clean laboratory and then re-dissolved in 5% HNO_3 . The concentrations of Al, Si, Na, Ca,
62 Mg, Sr, and Li in the leachate solutions were determined with an Agilent 4100 microwave
63 plasma atomic emission spectrometer (MP-AES) calibrated using synthetic standards. The
64 results are reported as nanomoles of element leached per gram of sample.

65 *Appendix A.2. Dissolved phase geochemical analyses*

66 Water samples were collected using slightly different methods depending upon the sam-
67 pling year. For samples collected before 2012, water was collected from the river surface
68 using a clean PP bottle, filtered on site with a $0.2 \mu\text{m}$ porosity nylon filter, and split into
69 two 60 mL high-density polyethylene bottles (HDPE). One of the 60 mL HDPE bottles was
70 preserved with 2 drops of high purity HCl dispensed from an acid-washed Teflon dropper
71 bottle for cation analyses. The other HDPE bottle was left unpreserved. In the laboratory,
72 samples with any remaining particulates (e.g., from flocculated aggregates forming after field
73 filtration) were re-filtered before analysis with a $0.2 \mu\text{m}$ nylon porosity filter.

74 After 2012, water samples were collected from the river surface with a clean PP bucket
75 and transferred to 10 L plastic bags before filtration. Within 24 hours of collection, the
76 samples were filtered with $0.2 \mu\text{m}$ porosity polyethersulfone (PES) filters housed in a teflon
77 filtration unit with a peristaltic pump and tygon tubing. The filtrate was collected directly
78 into two clean 60 mL HDPE bottles. One of the 60 mL HDPE bottle was preserved with 60
79 μL of concentrated distilled HNO_3 dispensed from a teflon vial with an acid-washed pipette
80 tip. The other HDPE bottle was left unpreserved.

81 *Appendix A.2.1. Cation and Si concentrations*

82 To determine the concentrations of Na, K, Ca, Mg, Si, Li, and Sr, the acidified water
83 samples were analyzed using an MP-AES calibrated with synthetic standards. Precision
84 and accuracy was assessed by analyzing a reference material every 15 samples. For Ca, Mg,
85 Na, K, and Si, the reference material ION-915 was used (Environment Canada). For Li,
86 the reference material TMDA-51.4 (Environment Canada) was used. For Sr, an in-house
87 prepared $SrCO_3$ solution was used. Replicate analyses of each solution reveals an analytical
88 precision within 5% (1σ) for each analyte.

89 *Appendix A.2.2. Anion concentrations*

90 To determine the concentrations of Cl^- and SO_4^{2-} , the un-acidified samples were ana-
91 lyzed with a Metrohm ion chromatograph equipped with a Metrosep A4/150 column and a
92 conductivity suppressor. The elements were eluted from the column with 3.2 mM Na_2CO_3
93 and 1.0 mM $NaHCO_3$ at a flow rate of 0.7 mL min^{-1} . The instrument was calibrated using
94 synthetic standards. Precision and accuracy was assessed by analyzing a certified reference
95 material (ION-915, Environment Canada) after every 15 samples. Replicate analyses of
96 ION-915 reveals an analytical precision within 5% (1σ) for each analyte.

97 *Appendix A.2.3. Sulfate-sulfur isotope measurements*

98 To measure the $\delta^{34}S_{V-CDT}$ of dissolved SO_4^{2-} , SO_4^{2-} was purified from \sim 1-10 mL of sam-
99 ple using either a cation or anion exchange resin following established protocols (Paris et al.,
100 2013). Before separation, all samples were evaporated to dryness within a clean laboratory.
101 For samples purified using a cation exchange resin, the sample residue was re-dissolved in
102 0.25 % HCl and introduced into a column containing Bio-Rad AG50X8 resin following Paris
103 et al. (2013). For sample purified using an anion exchange resin, the sample residue was
104 re-dissolved in 0.5 % HCl and introduced into a column of AG1X8 resin following Paris et al.
105 (2014). After elution from the columns, the samples were evaporated to dryness and then
106 re-dissolved in 5% HNO_3 . Before analysis, all samples were diluted and mixed with a sodium

107 solution to match the sodium and sulfate concentrations of the bracketing standard. The
108 samples were then analyzed using a Thermo Neptune Plus multi-collector inductively cou-
109 pled plasma mass spectrometer (MC-ICP-MS) at Caltech using sample-standard bracketing
110 to correct for instrumental drift and mass bias following Paris et al. (2013).

111 Replicate purification of sulfate and measurement of its sulfur isotopic composition from
112 select samples reveals variability of up to 0.2 ‰. This uncertainty value is reported in all
113 figures and tables but is not included after each value in the main text for brevity.

114 *Appendix A.2.4. Strontium isotope measurements*

115 To measure the radiogenic ($^{87}\text{Sr}/^{86}\text{Sr}$) isotopic composition of dissolved Sr, the acidi-
116 fied samples were purified using an automated HPLC separation with Sr Spec resin at the
117 Institute de Physique du Globe Paris (IPGP; Meynadier et al. 2006). The purified samples
118 were evaporated to dryness, re-dissolved in 0.5 M HNO_3 and analyzed on a Thermo Neptune
119 plus MC-ICP-MS at IPGP. A solution made from the NIST carbonate reference material
120 SRM987 was used to check accuracy regularly. To correct for Kr interference, the $^{83}\text{Kr}/^{84}\text{Kr}$
121 and $^{83}\text{Kr}/^{86}\text{Kr}$ ratios were determined using the blank solution at the beginning of the run
122 and the ^{83}Kr signal was monitored for each sample and standard. To correct for Rb inter-
123 ference, the ^{87}Rb signal of a 5 ppb Rb solution was measured at the beginning of the run
124 and the ^{85}Rb signal was monitored for each sample and standard.

125 The individual analytical uncertainty on each of the dissolved $^{87}\text{Sr}/^{86}\text{Sr}$ ratio measure-
126 ments is less than 0.1 permil. Nonetheless, given the large range of variability between
127 samples, the measured $^{87}\text{Sr}/^{86}\text{Sr}$ ratios are only be reported to three decimal places in the
128 main text.

129 *Appendix A.3. Inversion Model*

130 The inversion model is based on the mixing equation:

$$X/\Sigma_{measured}^+ = \sum_{f=1}^n F_f \times X/\Sigma_f^+ \quad (\text{A.1})$$

131 where $X/\Sigma_{measured}^+$ is a measured elemental ratio of element X, F_f is the fractional contribu-
 132 tion of end-member f, X/Σ_f^+ is the elemental ratio of end-member f, and n is the number of
 133 end-members. For isotopic ratios, we use the modified mixing equation:

$$\delta X_{measured} \times X/\Sigma_{measured}^+ = \sum_{f=1}^n F_f \times X/\Sigma_f^+ \times \delta X_f \quad (\text{A.2})$$

134 where $\delta X_{measured}$ is the measured isotopic ratio of element X and δX_f is the isotopic ratio of
 135 end-member f.

136 To perform the inversion, a single value for each end-member ratio (X/Σ_f^+ and δX_f) is
 137 randomly drawn from a predefined uniform distribution (see Table 1). Then, using these
 138 random end-member values and the measured ratios ($X/\Sigma_{measured}^+$ and $\delta X_{measured}$), the frac-
 139 tional contribution from each end-member (F_f) is calculated using the `mldivide` command in
 140 MATLAB 2015b. For each sample, we repeat this approach 6×10^4 times in order to ensure
 141 that a sufficient number of random end-member combinations are used so that the reported
 142 confidence intervals do not change appreciably between replicate calculations. If any of the
 143 calculated mixing fractions are negative, the results of that simulation are discarded. While
 144 this general approach applies to all of the mixing models, details specific to the different
 145 versions described in the main text are included below. The precise end-member definitions
 146 are included in Table 1.

147 *Appendix A.3.1. Na-Ca-Mg-Cl-SO₄- $\delta^{34}\text{S}$ inversion*

148 To apportion the solute budget between limestone, dolomite, granite, shale, rainfall, and
 149 evaporites, we use Cl/Σ^+ , Na/Σ^+ , Ca/Σ^+ , Mg/Σ^+ , SO_4/Σ^+ , and $\delta^{34}\text{S}$. With the added
 150 constraint that the fractional contributions from each end-member must all sum to one,
 151 this model includes 7 equations, which is one greater than the number required for 6 end-
 152 members. Consequently, we calculate a least squares solution for each simulation. Since
 153 some of the simulations calculated this way will have large errors, we calculate the sum of the
 154 squared residuals (SSE) for each simulation. For each sample, we calculate a reference SSE by

155 determining the 5th percentile value of SSE for all of the simulations for that sample. We then
156 select only the subset of simulations where the SSE is less than this reference value. Together,
157 all of the constraints result in an average of 224 valid simulations for each sample. For this
158 model, the *a posteriori* values of SO_4/Σ^+ for the carbonate and silicate end-members are
159 used to determine the proportions of sulfuric acid weathering for each sample. For reference,
160 the exact mixing model is included as a MATLAB script (`Torres_etal_A_inversion.m`).

161 *Appendix A.3.2. Na-Ca-Mg-Cl inversion*

162 To apportion the solute budget between limestone, dolomite, granite, shale, and rainfall,
163 we use Cl/Σ^+ , Na/Σ^+ , Ca/Σ^+ , and Mg/Σ^+ . With the added constraint that the fractional
164 contributions from each end-member must all sum to one, this model includes 5 equations.
165 Since the system is not over-constrained, we calculate an exact solution for each combination
166 of random end-members. Together, all of the constraints result in an average of 4649 valid
167 simulations for each sample. For reference, the exact mixing model is included as a MATLAB
168 script (`Torres_etal_B_inversion.m`).

169 *Appendix A.4. Sr isotope model*

170 For each simulation that produces a set of realistic mixing proportions, the predicted
171 Sr/Σ^+ and $^{87}\text{Sr}/^{86}\text{Sr}$ are calculated using equations A.1 and A.2. This calculation is repeated
172 1000 times using different end-member values for Sr/Σ^+ and $^{87}\text{Sr}/^{86}\text{Sr}$. Combinations of end-
173 members and mixing fractions that produce values of Sr/Σ^+ that are more than 5% from
174 the measured values are discarded. For reference, the exact mixing model is included as a
175 MATLAB script (`Torres_etal_C_inversion.m`).

176 *Appendix A.4.1. Li/ Σ^+ model*

177 For each calculation that produces a set of realistic mixing proportions, the Li/Σ^+ of the
178 sample is calculated using equation A.1. Only shale and granite are considered as Li sources.
179 To get Li/Σ^+ values for these end-members, we multiply the Li/Na ratios from Dellinger

180 et al. (2015) by the end-member Na/Σ^+ used in the simulation. For reference, the exact
181 mixing model is included as a MATLAB script (`Torres_etal_D_inversion.m`).

182 *Appendix A.5. Effect of weathering on $p\text{CO}_2$*

183 The fluxes of alkalinity and DIC delivered to the ocean by chemical weathering depend
184 upon the relative magnitude of different weathering reactions. Here, we consider how the
185 proportion of cations sourced from carbonate weathering and the proportion of total weath-
186 ering driven by sulfuric acid set the relative amounts of alkalinity and DIC production. By
187 defining reference ratios of alkalinity to DIC that are associated with no change in $p\text{CO}_2$,
188 we determine which combinations of weathering reactions increase or decrease atmospheric
189 $p\text{CO}_2$ over different timescales.

190 *Appendix A.5.1. Relevant Chemical Reactions*

191 To quantify the effects of different weathering reactions on the budgets of alkalinity
192 and DIC, we start by writing the acid consuming (carbonate and silicate dissolution) and
193 acid producing (carbonic acid disassociation and pyrite oxidation) half-reactions. We then
194 combine these half reactions in order to write full reactions for the weathering of carbonate
195 and silicate minerals by carbonic and sulfuric acids. Finally, by comparing the relative
196 amounts of DIC and alkalinity production resulting from each reaction, we determine how
197 the proportion of cations sourced from carbonate weathering and the proportion of total
198 weathering driven by sulfuric acid set the effect of weathering on atmospheric $p\text{CO}_2$ over
199 different timescales.

200 The half-reactions for the proton-promoted dissolution of carbonate and silicate minerals
201 can be written as:



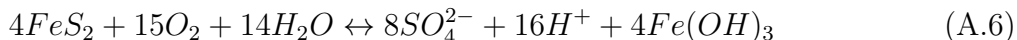
202 and



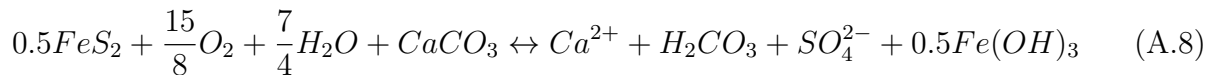
203 The corresponding half-reactions for acid generation by the disassociation of carbonic acid
 204 and the oxidation of pyrite can be written as:



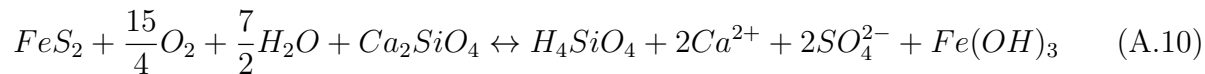
205 and



206 The acid consuming half reactions (carbonate and silicate dissolution) can be combined
 207 with the acid generating half reactions (carbonic acid disassociation and pyrite oxidation)
 208 to generate full reactions describing the weathering of carbonate and silicate minerals by
 209 carbonic and sulfuric acid. To do this, we combine the above equations with the assumption
 210 that the number of moles of protons generated and consumed should be equal. We also follow
 211 the convention of writing all species as the dominant species at the carbonic acid equivalence
 212 point. In particular, this means that we will write all DIC species as H_2CO_3 and balance
 213 reactions by adding H^+ ions as needed. The utility of this approach is that, after canceling
 214 out species that appear on both sides of an equation, any H_2CO_3 species that appear on the
 215 right hand side of an equation reflect DIC generation and any H^+ species that appear on
 216 the left hand side of an equation reflect alkalinity production. This approach yields the full
 217 equations:



218 and



219 for carbonate-carbonic, carbonate-sulfuric, silicate-carbonic, and silicate-sulfuric weathering
220 respectively.

221 To compare their effects on DIC and alkalinity, we normalize all of the full weathering
222 reactions (equations A.7 - A.10) by the charge equivalents of cations released, which is the
223 quantity shown in Table A.1. This normalization insures that the results are not sensitive
224 to the chosen mineral formula. This is particularly important for silicate minerals, which
225 typically contain cations other than Ca^{2+} in appreciable amounts. This normalization also
226 aids in the assessment of field data since estimates of chemical weathering in rivers are based
227 on measurements of cation release.

228 Using the coefficients in Table A.1, we can write equations for the production of alkalinity
229 and DIC by weathering where

$$Alkalinity = (z \times (0x + 0y)) + ((1 - z) \times (x + y)) \quad (A.11)$$

230 and

$$DIC = (z \times (0.5x + 0y)) + ((1 - z) \times (0.5x + 0y)) \quad (A.12)$$

231 with z being the proportion of weathering driven by sulfuric acid, x being the charge equiv-
232 alents of cations contributed by carbonate weathering, and y being the charge equivalents
233 of cations contributed by silicate weathering.

234 *Appendix A.5.2. Short Timescales*

235 In the modern ocean, the ratio of alkalinity to DIC is approximately one. Consequently,
236 on timescales shorter than the timescale associated with marine carbonate burial, atmo-
237 spheric pCO_2 will increase if the ratio of alkalinity to DIC delivered by rivers is less than

Table A.1: Alkalinity and DIC contributions per unit cation released (charge equivalents) for different weathering reactions

Mineral/Acid	ΔAlk	ΔDIC
Carbonate-Carbonic	1	0.5
Carbonate-Sulfuric	0	0.5
Silicate-Carbonic	1	0
Silicate-Sulfuric	0	0

1. We note that this is strictly valid for the modern oceanic alkalinity to DIC ratio. To graphically show the implied effects of different combinations of weathering reactions on atmospheric pCO_2 , we set equations A.11 and A.12 both equal to one in order to solve for parameter combinations that yield no change in atmospheric pCO_2 on short timescales, which gives the relationship

$$z_{short} = 1 - (0.5 \times R) \quad (\text{A.13})$$

where R is the proportion of cations sourced from carbonate weathering, i.e.:

$$R = \frac{x}{x + y} \quad (\text{A.14})$$

In a plot of R versus z (Figure 7), data that plot above the line described by Equation A.13 are associated with CO_2 release on timescales shorter than carbonate precipitation assuming close to modern conditions.

Appendix A.5.3. Long Timescales

Carbonate burial exports alkalinity and DIC from the ocean in a 2 to 1 ratio (reverse of equation A.7). So, on timescales longer than carbonate burial but shorter than pyrite burial ($< 10^7$ years; Berner and Berner 2012), atmospheric pCO_2 will increase if rivers deliver alkalinity and DIC to the ocean in a ratio that is less than 2. We suggest that this reference alkalinity to DIC ratio should be valid regardless of the oceanic alkalinity to DIC ratio. To graphically show the implied effects of different combinations of weathering reactions on atmospheric pCO_2 over long timescales, Equations A.11 and A.12 can be solved for when

255 Alk/DIC is equal to two, which gives the equation:

$$z_{long} = 1 - R \quad (\text{A.15})$$

256 In a plot of R versus z (Figure 7), data that plot above the line described by Equation A.15
257 are associated with pCO₂ increase on timescales longer than carbonate precipitation but
258 shorter than pyrite burial.

259

260

References

261 Berner, E.K., and Berner, R.A., 2012, Global environment: water, air, and geochemical
262 cycles: Princeton University Press.

263 Dellinger, M., Gaillardet, J., Bouchez, J., Calmels, D., Louvat, P., Dosseto, A., Gorge,
264 C., Alanoca, L., and Maurice, L., 2015, Riverine Li isotope fractionation in the Amazon
265 River basin controlled by the weathering regimes: *Geochimica et Cosmochimica Acta*,
266 doi:10.1016/j.gca.2015.04.042.

267 Gröger, J., Franke, J., Hamer, K., and Schulz, H.D., 2009, Quantitative recovery of elemental
268 sulfur and improved selectivity in a chromium-reducible sulfur distillation: *Geostandards
269 and Geoanalytical Research*, v. 33, p. 17–27, doi:10.1111/j.1751-908X.2009.00922.x.

270 Leleyter, L., and Probst, J., 1999, A new sequential extraction procedure for the speciation
271 of particulate trace elements in river sediments: *International Journal of Environmental
272 Analytical Chemistry*, v. 73, no. 2, p. 109–128.

273 Meynadier, L., Gorge, C., Birck, J.L., and Allègre, C.J., 2006, Automated separation of Sr
274 from natural water samples or carbonate rocks by high performance ion chromatography:
275 *Chemical Geology*, v. 227, no. 1-2, p. 26–36, doi:10.1016/j.chemgeo.2005.05.012.

276 Paris, G., Adkins, J.F., Sessions, A.L., Webb, S.M., and Fischer, W.W., 2014, Neoproterozoic
277 carbonate-associated sulfate records positive ³³S anomalies: *Science*, v. 346, no. 6210, p.
278 739–742.

279 Paris, G., Sessions, A.L., Subhas, A.V., and Adkins, J.F., 2013, MC-ICP-MS measurement
280 of $\delta^{34}\text{S}$ and $\Delta^{33}\text{S}$ in small amounts of dissolved sulfate: *Chemical Geology*, v. 345, p. 50–61,
281 doi:10.1016/j.chemgeo.2013.02.022.